Effect of re-melting strategies on the residual stresses in additively manufactured l-shaped IN718 parts

Prabhat Pant, Vladimir Luzin, Sebastian Proper, Seyed Hosseini, Johan Moverare, Kjell Simonsson, Ru Lin Peng

EFFECT OF RE-MELTING STRATEGIES ON THE RESIDUAL STRESSES IN ADDITIVELY MANUFACTURED L-SHAPED IN718 PARTS

Prabhat Pant[1]*, Vladimir Luzin[2], Sebastian Proper[3], Seyed Hosseini[3], Johan Moverare[1], Kjell Simonsson[1], Ru Lin Peng[1]

[1]*Dept. Of Management and Engineering, Linköping University, Sweden*

[2]*ANSTO, Australia,*[3]*RISE IVF AB, Sweden*

**Corresponding author: prabhat.pant@liu.se*

ABSTRACT

Manufacturing by the laser powder-based fusion (LPBF) method of additive manufacturing is in rising owing to the ease of the production of the complex shape metallic components. Optimization of the part's production and performance brings the issue of residual stresses (RS) thus, different processing ways are being investigated to minimize the level of RS within the window of the processing parameters such as laser speed, power, orientation, etc. Previously, it was shown that in-process remelting after every three printed layers showed a positive effect on reducing tensile surface residual stress for L-shaped part made of IN718. Using the aforementioned part as reference (RM-3), which used the same process parameters for both printing and remelting, three more parts were built with varying parameters for the remelting to compare the RS development. It was observed that keeping the energy density the same as for the RM-3 sample with a change in the laser power and scan speed resulted in increased surface tensile RS. A similar increment in RS was observed for the sample with increased energy density used for the remelting sequence. When the number of layers between the remelting sequence was reduced to one, only a slight increment in RS from the RM-3 sample was observed.

Keywords: Residual stress, Neutron diffraction, additive manufacturing; scan strategy; IN718

1. Introduction

Laser-based powder bed fusion (LPBF) method is one of the common methods implemented in the realm of additive manufacturing (AM) technology to fabricate highly complex design components. This process relies on the laser beam scanning particular areas in the powder bed which is given as input from a CAD geometry in a layer after layer sequence. Due to this repeated process of laser melting, the temperature between the subsequent layers differs vastly due to high cooling rates in the order of 10^5 -10^6 K/s [1]. This thermal mismatch between already printed layers and freshly printed layer causes the development of residual stress (RS) during the process. The magnitude of the RS generated varies with processing parameters such as laser power, speed, laser scan strategy, material system, part orientation, etc. Previously, high levels of tensile stresses close to the yield strength of the material were observed at the surface [2] and these high levels of stress being generated can lead to the formation of cracks during printing as well as warping of the part [3–5], causing failure of the part while printing or leading to sub-optimal parts in terms of mechanical performance. It is well known that the magnitude of RS can affect the in-service life drastically especially in dynamic loading conditions. These RS are in an equilibrium state when no external loads are applied. However, when external mechanical loads are applied the RS can elevate or degrade the mechanical performance of the

* Corresponding author. Prabhat.pant@liu.se

component depending upon their magnitude and distribution. It is a known phenomenon that tensile surface RS can reduce the fatigue life of the component by assisting surface crack opening, and growth [6–9] and the opposite is true for compressive surface RS which will deter the crack growth and thus increase the fatigue life [7–10]. In the best-case scenario, compressive RS at the surface or low level of tensile RS are desired.

LPBF process provides significant freedom in terms of the selection of processing parameters to produce high-quality products. As mentioned earlier that temperature gradient is one of the main mechanisms to form RS, so the process parameters used can significantly alter the RS magnitude. Out of many laser scan strategies, the most common one is to employ a 67° rotation of laser movement between the layers to have a high-density part, to lower the degree of texture as well as to have a lower magnitude of the RS [11–14]. Also, the orientation of the part in the build plate and their placement in the build plate affect the RS magnitude for the same scan strategy employed for all the components [2,15–19]. Generally, using a shorter scan length has shown lower RS formation [20]. Similarly, non-standard strategies such as fractal scans had shown promising results in printing non-weldable superalloys which are highly susceptible to cracking [21].

Out of various scan strategies, remelting strategy where already printed layers are scanned again with the laser but without any new layer of powder being applied on top can modify the RS magnitude in as-built components. In an earlier study by Shiomi et al. [22] on 316L stainless steel, it was reported that re-scanning an already printed layer with 150 % higher power than that used for printing reduced the RS by approximately 55 %. Changing the scan speed for rescanning can also affect the final RS magnitude and it had been reported that using a higher speed led to increased RS levels [23]. For IN718, using 5% of the energy density used for normal printing for rescanning every layer resulted in a reduction of RS [24]. Also, it has been reported that remelting every 3rd layer with the same power used for the primary printing resulted in approximately 25 % lower tensile RS at the surfaces [12]. To manufacture high-value complex components, fine-tuning of the process parameters depending upon geometry and the material being used is required. In the current work, the investigation is focused on the influence of different process parameters used for remelting sequences for L-shaped samples manufactured using LPBF technology.

1.1. Material and Method

Samples from gas atomized Inconel 718 (IN718) powder with 10–45 µm particle size were printed using an SLM 125 HL (SLM Solutions Group AG, Germany) machine equipped with a soft rubber re-coater system and Argon was used as protective gas. In this study, L-shaped samples as shown in Fig. 1 were printed using four different scanning techniques for remelting. For primary printing of layers for all the samples, a strategy with 67° rotation of laser path between the layers was employed. The layer thickness was kept at 30 microns and a laser hatch distance of 0.12 mm was used. Stainless steel 316L was used as the build plate and the temperature of the build plate was kept at 200° C. In total 8 samples were printed, 2 for each scanning strategy. One set of samples was used to create a sliced sample for the measurement of the stress-free lattice parameter. The reference sample (RM-3) was manufactured employing a remelting scan after every 3rd printed layer with the same process parameters as the primary printing. Details of samples printed for the current study together with respective parameters can be found in Table 1.

Table 1 Samples and parameters used for printing

	Power (W)	Speed (mm/s)	Energy density (ED) (J/mm^3)	Remarks
Primary printing	200	900	61.7	Same for all the samples
RM-3	200	900	61.7	Remelting every 3rd layer with the same strategy as for primary printing
RM-P	***300***	***1350***	61.7	Remelting every layer with higher speed and power but the same ED
RM-ED	***300***	900	***92.59***	Energy density changed and remelting was done every 3rd layer
RM-1	200	900	61.7	Remelting done every layer with same ED as RM-3

The RS were measured using the neutron diffraction technique at the KOWARI beamline of ANSTO. The neutron diffraction method relies on using a particular set of *hkl* planes as a strain gauge and change in distance between the planes d_{hkl} due to the RS is measured using Braggs law [25]. This measured distance is converted into strains using a stress-free sample where the same *hkl* planes are measured. For the current study *311* planes were measured as IN718 is FCC dominant material and this plane is least affected by texture and has high intensity as well [25]. Strains were measured parallel to the sample axes X, Y, and Z at four cross-sections as shown in Fig. 1. The stress components along these axes were calculated using elastic isotropy Hooke's law and elastic constant values for the *311* plane: E_{311} = 202 GPa and ν_{311} = 0.31 from [26]. Uncertainty for the stress values calculated for each point was ~30 MPa. Details regarding experimental setup and the stress-free sample measurement and stress (force) balance in the cross-section can be found in [12].

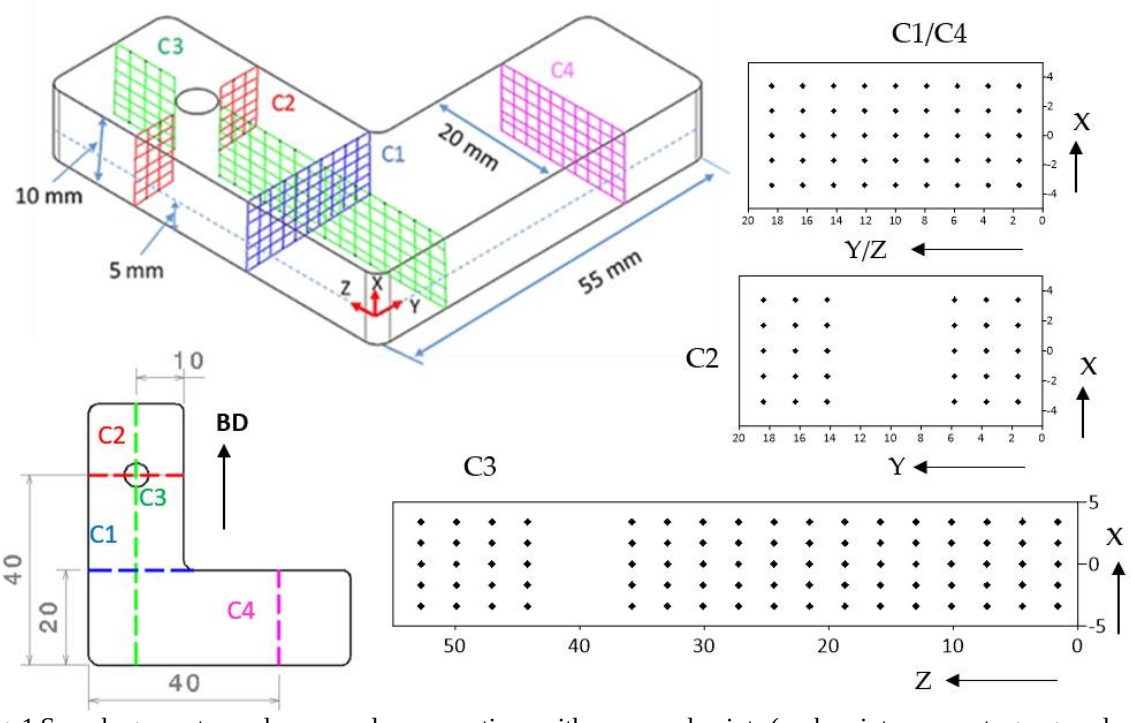

Fig. 1 Sample geometry and measured cross-sections with measured points (each point represents gauge volume size of 2 x 2 x 2 mm^3)

2. Results and Discussion

Results from the neutron diffraction measurements are presented in Fig. 2 for the cross-sections C1 and C2 in the different samples. For σ_z along the build direction (BD), tensile stresses near the surface are revealed, with a gradual change towards a compressive field in the center of the cross-sections for all the measured samples. Similar stress distributions with a stress magnitude between 600 - 850 MPa near the surface and about -600 MPa in the central region are observed for all the samples. For the C2 cross-section, the tensile stresses are in general somewhat higher due to the presence of the hole. On the other hand, low tensile stresses near the surface, around 200 MPa, and compressive stresses of similar magnitude in the center region are observed for both σ_y and σ_x which are in the transverse (Y) and through-thickness (X) direction, respectively.

It is evident that keeping the energy density (ED) the same but increasing laser speed and power for the remelting sequence resulted in higher tensile stresses in BD in the RM-P sample in comparison to the reference sample (RM-3). This tensile stress increased by approximately 200 MPa and 150 MPa near the surface is observed in the C1 and C2 cross-sections, respectively. From Fig. 2 looking into sample RM-ED, increasing the energy density also gave higher stress in BD near the surface for both C1 and C2 cross-sections but in contrast to the RM-P sample a slightly lower increment was observed in C1, and a higher increment was observed in C2. When the remelting was performed on every layer in RM-1, no big variation in stress distribution and magnitude was found for the C2 cross-section but a slight increment in the C1 cross-section for the BD in comparison to the RM-3 sample. For the other stress components for all the samples, no significant variation in stress distribution was observed for C1 and C2 cross-sections.

Looking into the other two cross-sections, C3 and C4 (see Fig. 3 and Fig. 4), also reveals a stress change from tensile to compressive with moving from the outer surface towards the bulk of the cross-sections. Both the cross-sections in samples RM-P, RM-ED, and RM1 showed slightly lower values of stresses near the base plate (at Z=0) for the σ_y which is perpendicular to the cross-section. Higher stress levels of approximately 400 MPa and 200 MPa were observed near the top surfaces, Z= 55 mm, and 20 mm for C3 and C4 respectively. Similarly, a very low level of tensile stress is observed for σ_z close to the base plate for RM-P, RM-ED, and RM-1, and a greater region of higher compressive stress is seen in comparison to the RM-3 sample. As for σ_x, no big variation in stress distribution is observed in both the cross-sections between the samples and therefore are not presented here.

Remelting every 3rd layer (RM-3) using the same parameters as for the primary printing reduced the surface tensile stresses by approximately 25 % as mentioned earlier [12]. This is because one of the primary reasons for RS formation in AM is due to the temperature gradient between the consecutive layers and the temperature gradient between the layers is decreased as the remelting will elevate the temperature of the already cooled layer to a higher level and thus reduce the thermal strain developed during processing. Changing the laser power and scan speed while keeping the rest of the remelting parameters unchanged has modified the magnitude of the RS. This phenomenon can be linked to the difference in the resulting temperature rise of the solidified layers by the remelting sequence or cooling rate. In the case of the RM-P sample, both the laser power and speed were increased for the remelting sequence. Although the total energy input was the same as for the RM-3, due to the higher scan speed, heat conduction from the melt pool to the already solidified layers and bulk was quicker, resulting in higher thermal strains which created the higher magnitude of RS. In the case of the RM-ED sample, a higher energy input due to the increment in laser power led to more heat accumulation, leading to a greater heat-affected zone. Due to the slower scan speed, the heat accumulated gets dissipated to the bulk more gradually than in the RM-P sample so the change increment in RS is slightly lower than in the RM-P case, but the distribution remains the same. In the case of the sample without

any remelting utilized, the effect of increasing energy density has been studied earlier and it has been reported that increasing energy density is not beneficial from the point of view of RS [27–29].

Remelting every layer (RM-1) did not show any significant change in RS magnitude and distribution in comparison to the RM-3 sample. In principle remelting every layer should increase the temperature of the already printed layers higher than doing it after every 3rd layer but from the observation, there is no strong evidence to suggest that. This can be due to the use of the same energy density for both cases and this leads to the same penetration depth which is typically between 3 – 4 layers. Thus, the heat affect zone will be similar. So, from point of view of reducing the time for printing remelting should be done based on the number of layers the laser can penetrate with one set of parameters.

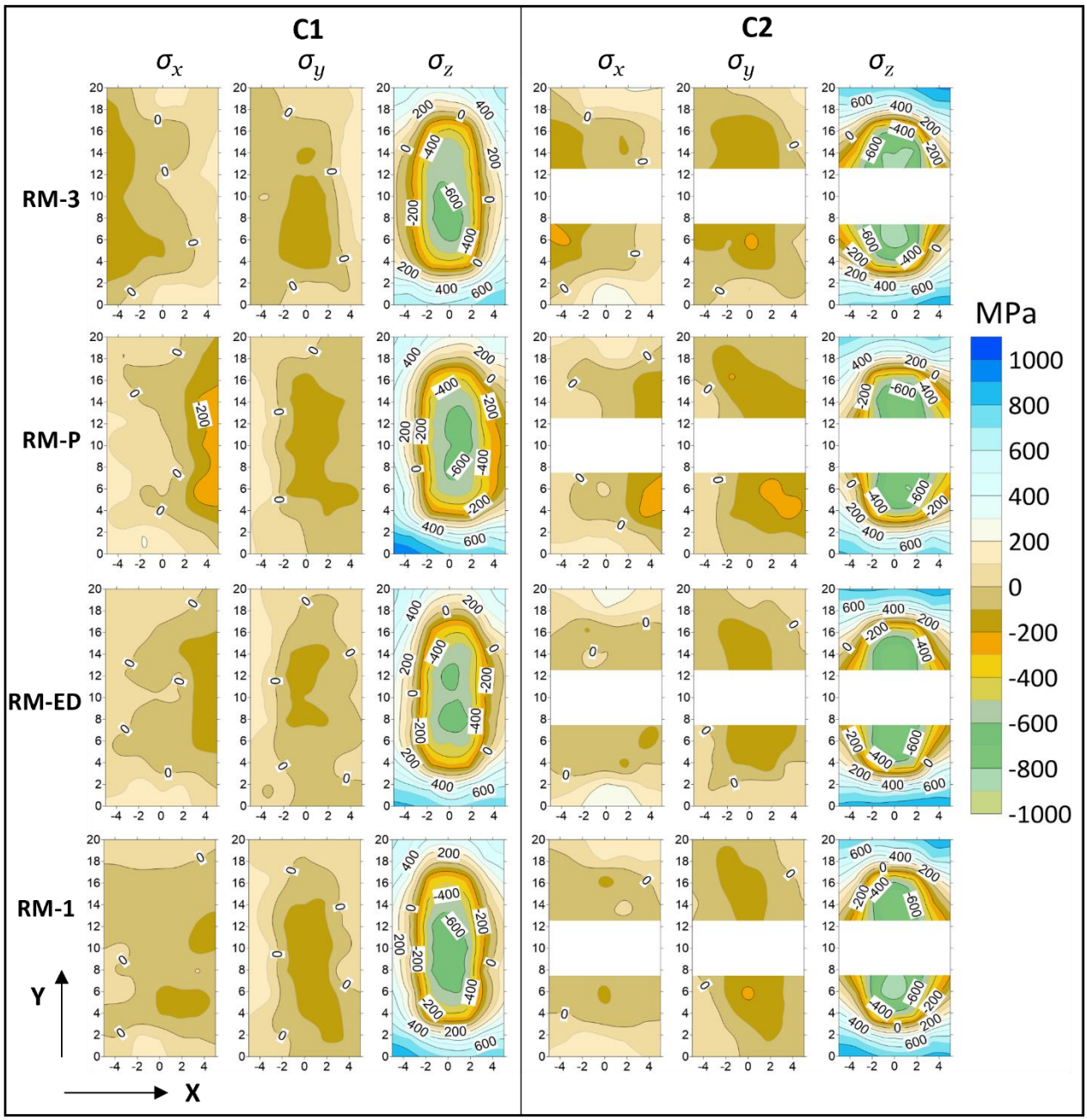

Fig. 2 Measured stress distribution for different samples for C1 and C2 cross-sections

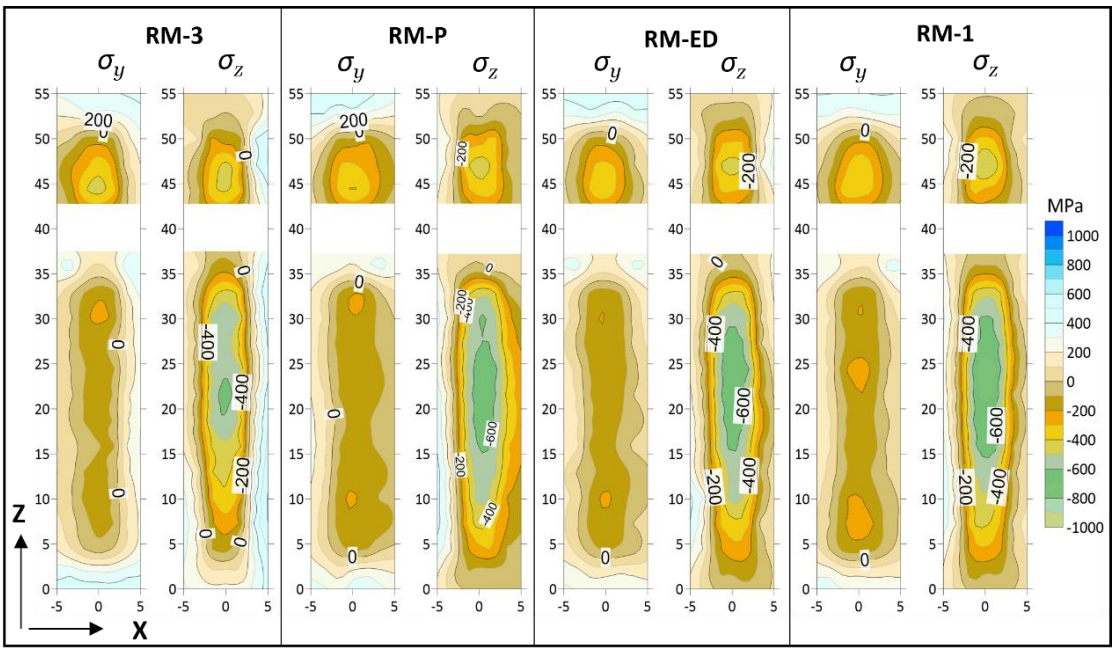

Fig. 3 Stress distribution for C3 cross-section

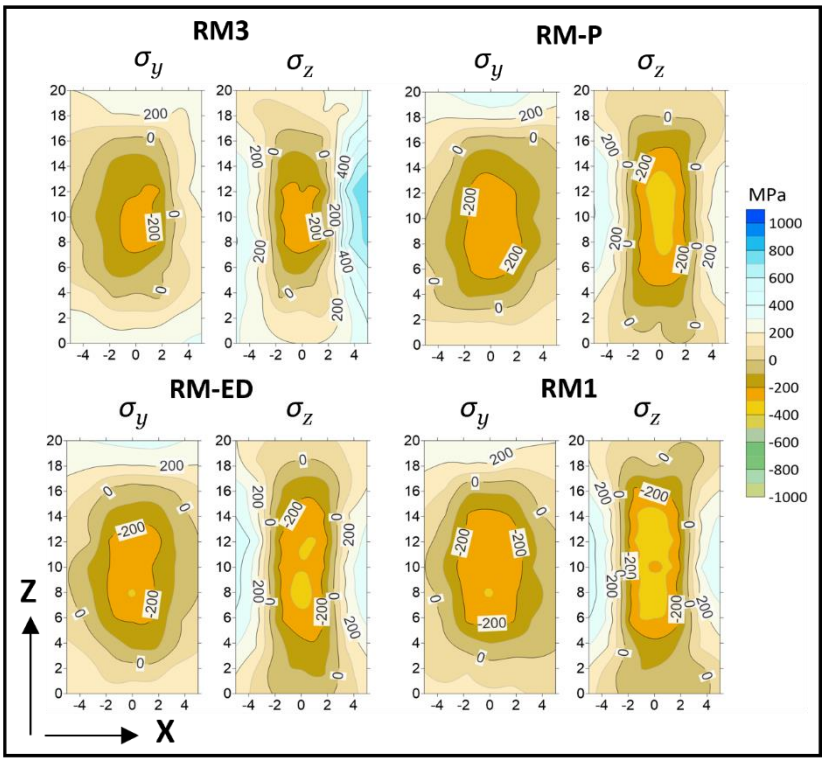

Fig. 4 Stress distribution for C4 cross-section

3. Conclusion:

With remelting, RS can be reduced in comparison to the normal printing with the same parameters, but careful selection of remelting parameters is important to achieve the desired reduction in surface RS. Here it was observed that the same energy density but with higher speed and power used for the remelting can increase the RS levels at the surface in the building direction. Similar nature of RS distribution and magnitude was also observed for samples with higher energy density for the remelting scan. In addition, remelting at every printed layer does not

seem to have any positive influence on decreasing the RS levels. While this study demonstrates the dependence of RS on processing parameters for the re-melting strategy (RM), more comprehensive investigation is required to fine-tune and identify the optimum process parameters such as scan strategy, power, speed, number of layers after which re-melting is to be done, etc., for remelting to be adopted as one of the methods to reduce the RS in as-built samples.

Acknowledgments

This research is funded by the Swedish Foundation for Strategic Research (SSF) within the Swedish national graduate school in neutron scattering (SwedNess) (grant number GSn15–0008). The neutron diffraction experiments were conducted at Australia Nuclear Science and Technology Organization's (ANSTO) KOWARI beamline through proposals 8337 and 8933. The authors gratefully acknowledge the support provided by the ANSTO during the experiment. The Additive Manufacturing Research Laboratory (AMRL) at RISE IVF is acknowledged for manufacturing all the specimens.

References

[1] D. Gu, Y.C. Hagedorn, W. Meiners, G. Meng, R.J.S. Batista, K. Wissenbach, R. Poprawe, Densification behavior, microstructure evolution, and wear performance of selective laser melting processed commercially pure titanium, Acta Mater. 60 (2012) 3849–3860. https://doi.org/10.1016/j.actamat.2012.04.006.

[2] P. Pant, S. Proper, V. Luzin, S. Sjöström, K. Simonsson, J. Moverare, S. Hosseini, V. Pacheco, R.L. Peng, Mapping of residual stresses in as-built Inconel 718 fabricated by laser powder bed fusion: A neutron diffraction study of build orientation influence on residual stresses, Addit. Manuf. 36 (2020) 101501. https://doi.org/10.1016/j.addma.2020.101501.

[3] D. Buchbinder, W. Meiners, N. Pirch, K. Wissenbach, J. Schrage, Investigation on reducing distortion by preheating during manufacture of aluminum components using selective laser melting, J. Laser Appl. 26 (2014) 012004. https://doi.org/10.2351/1.4828755.

[4] L.N. Carter, C. Martin, P.J. Withers, M.M. Attallah, The influence of the laser scan strategy on grain structure and cracking behaviour in SLM powder-bed fabricated nickel superalloy, J. Alloys Compd. 615 (2014) 338–347. https://doi.org/10.1016/j.jallcom.2014.06.172.

[5] P. Mercelis, J.P.J.-P.J. Kruth, Residual stresses in selective laser sintering and selective laser melting, Rapid Prototyp. J. 12 (2006) 254–265. https://doi.org/10.1108/13552540610707013.

[6] Y. Hua, Z. Liu, Experimental investigation of principal residual stress and fatigue performance for turned nickel-based superalloy Inconel 718, Materials (Basel). 11 (2018). https://doi.org/10.3390/ma11060879.

[7] G.A. Webster, A.N. Ezeilo, Residual stress distributions and their influence on fatigue lifetimes, Int. J. Fatigue. 23 (2001) 375–383. https://doi.org/10.1016/s0142-1123(01)00133-5.

[8] H. Köhler, K. Partes, J.R. Kornmeier, F. Vollertsen, Residual Stresses in Steel Specimens Induced by Laser Cladding and their Effect on Fatigue Strength, in: Phys. Procedia, 2012. https://doi.org/10.1016/j.phpro.2012.10.048.

[9] M.N. James, D.J. Hughes, Z. Chen, H. Lombard, D.G. Hattingh, D. Asquith, J.R. Yates, P.J. Webster, Residual stresses and fatigue performance, Eng. Fail. Anal. 14 (2007) 384–395. https://doi.org/10.1016/j.engfailanal.2006.02.011.

[10] Z. Chen, R. Lin Peng, J. Moverare, O. Widman, D. Gustafsson, S. Johansson, Effect of Cooling and Shot Peening on Residual Stresses and Fatigue Performance of Milled Inconel 718, in: Residual Stress. 2016, 2017: pp. 13–18. https://doi.org/10.21741/9781945291173-3.

[11] B. Cheng, S. Shrestha, K. Chou, Stress and deformation evaluations of scanning strategy effect in selective laser melting, Addit. Manuf. 12 (2016) 240–251. https://doi.org/10.1016/j.addma.2016.05.007.

[12] P. Pant, F. Salvemini, S. Proper, V. Luzin, K. Simonsson, S. Sjöström, S. Hosseini, R. Lin Peng, J. Moverare, A study of the influence of novel scan strategies on residual stress and microstructure of L-shaped LPBF IN718 samples, Mater. Des. 214 (2022) 110386.

https://doi.org/10.1016/j.matdes.2022.110386.

[13] N. Nadammal, S. Cabeza, T. Mishurova, T. Thiede, A. Kromm, C. Seyfert, L. Farahbod, C. Haberland, J.A. Schneider, P.D. Portella, G. Bruno, Effect of hatch length on the development of microstructure, texture and residual stresses in selective laser melted superalloy Inconel 718, Mater. Des. 134 (2017) 139–150. https://doi.org/10.1016/j.matdes.2017.08.049.

[14] J.H. Robinson, I. Robert, T. Ashton, E. Jones, P. Fox, C. Sutcliffe, The effect of hatch angle rotation on parts manufactured using selective laser melting, (n.d.). https://doi.org/10.1108/RPJ-06-2017-0111.

[15] A. Salmi, G. Piscopo, E. Atzeni, P. Minetola, L. Iuliano, On the Effect of Part Orientation on Stress Distribution in AlSi10Mg Specimens Fabricated by Laser Powder Bed Fusion (L-PBF), Procedia CIRP. 67 (2018) 191–196. https://doi.org/10.1016/j.procir.2017.12.198.

[16] A.S. Wu, D.W. Brown, M. Kumar, G.F. Gallegos, W.E. King, An Experimental Investigation into Additive Manufacturing-Induced Residual Stresses in 316L Stainless Steel, Metall. Mater. Trans. A. 45 (2014) 6260–6270. https://doi.org/10.1007/s11661-014-2549-x.

[17] L. Mugwagwa, D. Dimitrov, S. Matope, T. Becker, A methodology to evaluate the influence of part geometry on residual stresses in selective laser melting, in: Int. Conf. Compet. Manuf., 2016: pp. 133–139.

[18] B. Vrancken, V. Cain, R. Knutsen, J. Van Humbeeck, Residual stress via the contour method in compact tension specimens produced via selective laser melting, Scr. Mater. 87 (2014) 29–32. https://doi.org/10.1016/j.scriptamat.2014.05.016.

[19] T. Mishurova, K. Artzt, J. Haubrich, G. Requena, G. Bruno, New aspects about the search for the most relevant parameters optimizing SLM materials, Addit. Manuf. 25 (2019) 325–334. https://doi.org/10.1016/j.addma.2018.11.023.

[20] Y. Lu, S. Wu, Y. Gan, T. Huang, C. Yang, L. Junjie, J. Lin, Study on the microstructure, mechanical property and residual stress of SLM Inconel-718 alloy manufactured by differing island scanning strategy, Opt. Laser Technol. 75 (2015) 197–206. https://doi.org/10.1016/j.optlastec.2015.07.009.

[21] S. Catchpole-Smith, N. Aboulkhair, L. Parry, C. Tuck, I.A. Ashcroft, A. Clare, Fractal scan strategies for selective laser melting of 'unweldable' nickel superalloys, Addit. Manuf. 15 (2017) 113–122. https://doi.org/10.1016/j.addma.2017.02.002.

[22] M. Shiomi, K. Osakada, K. Nakamura, T. Yamashita, F. Abe, Residual Stress within Metallic Model Made by Selective Laser Melting Process, CIRP Ann. 53 (2004) 195–198. https://doi.org/10.1016/S0007-8506(07)60677-5.

[23] J.-P.P. Kruth, J. Deckers, E. Yasa, R. Wauthlé, Assessing and comparing influencing factors of residual stresses in selective laser melting using a novel analysis method, Proc. Inst. Mech. Eng. Part B J. Eng. Manuf. 226 (2012) 980–991. https://doi.org/10.1177/0954405412437085.

[24] J.H. Park, G.B. Bang, K.-A. Lee, Y. Son, W.R. Kim, H.G. Kim, Effect on microstructural and mechanical properties of Inconel 718 superalloy fabricated by selective laser melting with rescanning by low energy density, J. Mater. Res. Technol. 10 (2021) 785–796. https://doi.org/10.1016/j.jmrt.2020.12.053.

[25] M.T.M.T. Hutchings, P.J. Withers, T.M. Holden, T. Lorentzen, Introduction to the Characterization of Residual Stress by Neutron Diffraction, CRC Press, 2005. https://doi.org/10.1201/9780203402818.

[26] P.E. Aba-Perea, T. Pirling, P.J. Withers, J. Kelleher, S. Kabra, M. Preuss, Determination of the high temperature elastic properties and diffraction elastic constants of Ni-base superalloys, Mater. Des. 89 (2016) 856–863. https://doi.org/10.1016/j.matdes.2015.09.152.

[27] T. Simson, A. Emmel, A. Dwars, J. Böhm, Residual stress measurements on AISI 316L samples manufactured by selective laser melting, Addit. Manuf. 17 (2017) 183–189. https://doi.org/10.1016/j.addma.2017.07.007.

[28] G. Vastola, G. Zhang, Q.X. Pei, Y.-W.W. Zhang, Controlling of residual stress in additive manufacturing of Ti6Al4V by finite element modeling, Addit. Manuf. 12 (2016) 231–239. https://doi.org/10.1016/j.addma.2016.05.010.

[29] T. Mukherjee, V. Manvatkar, A. De, T. DebRoy, Mitigation of thermal distortion during additive manufacturing, Scr. Mater. 127 (2017) 79–83. https://doi.org/10.1016/j.scriptamat.2016.09.001.